Journal of Molecular Modeling (2023) 29:170
https://doi.org/10.1007/s00894-023-05567-8

ORIGINAL PAPER

Tailoring and functionalizing the graphitic-like GaN and GaP nanostructures as selective sensors for NO, NO_2, and NH_3 adsorbing: a DFT study

Fatemeh Mollaamin[1] · **Majid Monajjemi**[2]

Received: 19 March 2023 / Accepted: 19 April 2023 / Published online: 6 May 2023

Abstract

Context Langmuir adsorption of gas molecules of NO, NO_2, and NH_3 on the graphitic GaN and GaP sheets has been accomplished using density functional theory. The changes of charge density have shown a more important charge transfer for GaN compared to GaP which acts both as the electron donor while gas molecules act as the stronger electron acceptors through adsorption on the graphitic-like GaN surface. The adsorption of NO and NO_2 molecules introduced spin polarization in the PL-GaN sheet, indicating that it can be employed as a magnetic gas sensor for NO and NO_2 sensing.

Methods The partial electron density states based on "PDOS" graphs have explained that the NO and NO_2 states in both of GaN and GaP nanosheets, respectively, have more of the conduction band between − 5 and − 10 eV, while expanded contribution of phosphorus states is close to gallium states, but nitrogen and oxygen states have minor contributions. GaN and GaP nanosheets represent having enough capability for adsorbing gases of NO, NO_2, and NH_3 through charge transfer from nitrogen atom and oxygen atom to the gallium element owing to intra-atomic and interatomic interactions. Ga sites in GaN and GaP nanosheets have higher interaction energy from Van der Waals' forces with gas molecules.

Keywords Gas sensor · Gallium nitride (GaN) · Gallium phosphide (GaP) · NO · NO_2 · NH_3 · Sensitivity · DFT · Langmuir adsorption

Introduction

Generally gas sensors are largely approved with the properties such as high selectivity and sensitivity, low cost, small size, long working life, and resistant activity in the different environmental status [1–3]. Based on application of graphene as gas sensor in some works [4–6], it has been confirmed that the charge transfer diffused by adsorbing of gas molecules on the graphene surface might be considered to produce sensitive detectors. Moreover, sensor attributes can change the resistance of the graphene nanosheet once the gas molecules act like acceptors or donors of electrons.

✉ Fatemeh Mollaamin
smollaamin@gmail.com

[1] Department of Biology, Faculty of Science, Kastamonu University, Kastamonu, Turkey

[2] Department of Chemical Engineering, Central Tehran Branch, Islamic Azad University, Tehran, Iran

Different usages of carbon nanocompounds, such as adsorbing of hydrogen, hazardous compounds, and gas and designing the sensor instruments [7–16]. Recently, many materials including carbon nanostructures have been designed and applied as adsorptive removal of environmental pollutant gases [17–19]. Thus, it is essential to make high-implement gas detectors for distinguishing hazardous gases. In addition, enough implanting of the carbon nanostructures with transition metals might enhance their adsorbing ability and adjust their adsorbing selectivity as the excellent dopant applicants. The gas sensors containing metal oxides have been used to recognize hazardous pollutant gases having most of gas sensing characteristics except accurate selectivity [20]. Their detecting mechanism usually deals with the chemical interaction between the gas molecule and the oxygen molecule adsorbed on the surface, because cross sensitivity among various analyte gas compounds is obvious in a metal oxide-based sensor instrument [21, 22]. For example, the reconnaissance of SO_2 and NO_2 molecules is prevented due to cross-interference when diffused in a mixed status from a static origin [23]. Moreover,

Clark and his co-workers have investigated the noncovalent interactions due to chemical interpretation and analyses of bonding interactions by using the Hellmann–Feynman which connects the gap between quantum mechanics and conceptual chemistry [24]. These issued can be interpreted in coulombic terms, polarization and electrostatics, and which include electronic correlation and dispersion [24].

Recently, two-dimensional nanomaterials with high surface and large like phosphorene and silicene have known efficient in gas detecting, which can largely transfer the charge density between gas molecules and the substrates [25–28].

Semiconductor materials are mainly prepared from the elements in groups II to VI of the periodic table [29]. The compound in the groups III–V, each atom of group III is bonded to four atoms of group V for attaining an octet in the valence band, when the valence charge from an atom of group V transfers toward an atom of group III and cultivates partial ionic bonding to the crystal surface [30].

The GaN structure is one of the most discovered group III-nitride semiconductors which have been applied in different applications like electronic and optoelectronic devices and sensor instruments [31–34]. Considering the prominent electronic properties of gallium nitride (GaN), it can be an appropriate case for gas sensing [35–41]. For instance, some studies have exhibited that $Ga_{12}N_{12}$ nanoclusters are capable for gas sensing of CO, NO, NO_2, and HCN gas molecules [37, 38]. Moreover, GaN nanostructures suggest firm action under different radiation and in space conditions at room-temperature and wide varieties of temperature and humidity as compared to metal-oxides [42]. In addition, it has been investigated that magnetic properties instead of electrical properties owing to the interaction between gas molecule and surface in the active compound, the PL-GaN sheet could be applied as a largely selective magnetic gas detector for NO and NO_2 sensing [40, 41]. DFT computations have accomplished and indicated that GaN wurtzoids as an agent of GaN nanocrystals are appropriate for hydrogen detecting nanostructures. The nitrogen sites were discovered to have the function for the hydrogen sensing susceptibility. It is obvious that wurtzoids are bundles of capped (3, 0) nanotubes that build the wurtzite phase when they attain nanocrystal or bulk sizes [43].

Moreover, GaP has been investigated as a sensitive material for construction of anodically bonded cells for atomic detectors because of its properties containing optical transparency in the near "IR" and high thermal conductivity make it a notable option in sensor devices [44].

One-dimensional semiconductor nanowires often consist of polytypic structures, due to the coexistence of various crystal GaAs as the semiconductors by using the chemical vapor transport approach [45]. Concerning damaging impact of NO_2 on human health and environment makes NO_2 gas sensors, and their state-of-the-art characteristics have been studied [46–48].

Ammonia "NH_3", which is an important ingredient of reactive nitrogen, participates in prevalent harmful impacts on health. Nitrogen atom in NH_3 helps to form the atmospheric aerosols which remain in the atmosphere for some days [49–51]. Moreover, "NH_3" is very crucial in biology and medicine as well as in environmental controlling equipment. Recently, GaP epitaxial nanowires have been investigated as efficient adsorption material of NH_3 detection with a simple device [52].

Therefore, this research wants to investigate the adsorption of hazardous gas of NO, NO_2, and NH_3 by using monolayer graphitic GaN and GaP nanosheets with an atomically flat planar honeycomb hexagonal structure as "PL-GaN" [53–55] employing density functional theory (DFT) to discover the adsorbing parameters of the GaN and GaP nanosheets.

Theoretical Insights, applied material, and method

In this research, the simulated calculations have been directed in the GaussView 6.06.16 [56] and calculated by Gaussian 16, Revision C.01 [57] using the DFT method. The [Perdew–Burke–Ernzerhof] "PBE" functional with high-precision generalized gradient approximation "GGA" has been employed to achieve more authentic results [58]. Every simulated group contains a graphitic-like of length 25 Å with bond length of 1.95 Å for GaN and 2.28 Å for GaP with a single NO, NO_2, or NH_3 molecule adsorbed onto it (Scheme 1).

The charge transfer between adsorbates of NO, NO_2, and NH_3 and adsorbents of GaN and GaP nanosheets is calculated due to the Bader charge analysis [59]. This method can measure charge accumulation from the charge of each atom in the complex model. Finally, the total adsorption charge transfer can be obtained as formula: $\Delta Q_t = Q_2 — Q_1$, where Q_2 and Q_1 remark the charge of NO, NO_2, and NH_3 before and after adoption, respectively. As a matter of fact, positive ΔQ_t indicates that electrons are transferred from gas molecules of NO, NO_2, and NH_3 to the surfaces of GaN and GaP nanosheets, and the adsorbent acts as an electron acceptor [60, 61].

The adsorbing of NO, NO_2, and NH_3 gases on the surfaces of GaN and GaP nanosheets was defined by the theory "Langmuir" isotherm [62–65], which indicates the chemisorption between gas molecules and GaN and GaP surfaces. The adsorbates of NO, NO_2, and NH_3 molecules are maintained on surfaces of GaN and GaP with "Langmuir" chemisorption (Scheme 1).

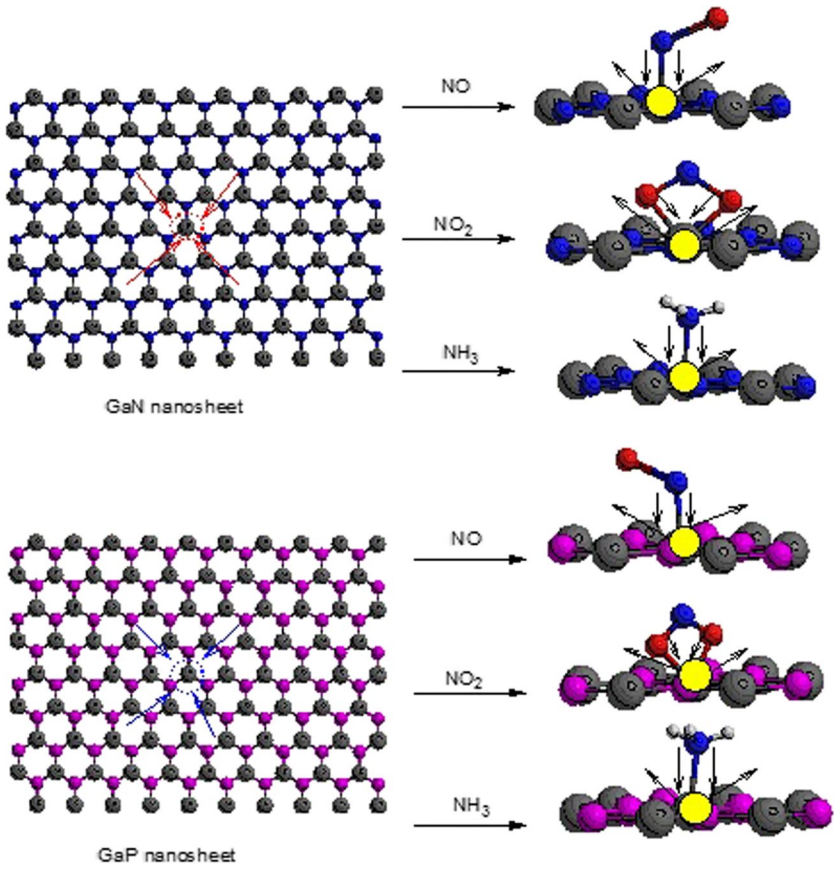

Scheme 1 "Langmuir" adsorption of NO, NO_2, and NH_3 onto GaN and GaP nanosheets

The changes of charge density analysis in the adsorption process has illustrated that GaN nanosheet shows the Bader charge of − 1.382e, before adsorption of NO, NO_2, and NH_3, and − 0.598 e, − 0.904e, − 0.625e, after adsorption of NO, NO_2, and NH_3, respectively. In addition, GaP nanosheet shows the Bader charge of − 0.721e, before adsorption of NO, NO_2, and NH_3, and − 0.183e, − 0.352e, − 0.462e, after adsorption of NO, NO_2, and NH_3, respectively.

Therefore, the changes of charge density for "Langmuir" adsorption of NO, NO_2, and NH_3 on GaN surface alternatively are $\Delta Q_{NO\rightarrow GaN} = +0.784^{>} \Delta Q_{NH3\rightarrow GaN} = +0.757^{>} \Delta Q_{NO2\rightarrow GaN} = 0.478$.

In addition, the changes of charge density for "Langmuir" adsorption of NO, NO_2, and NH_3 on GaP surface alternatively are $\Delta Q_{NO\rightarrow GaP} = +0.538^{>} \Delta Q_{NO2\rightarrow GaP} = +0.369^{>} \Delta Q_{NH3\rightarrow GaP} = 0.259$.

The values of changes of charge density have shown a more important charge transfer for GaN compared to GaP which acts both as the electron donor while gas molecules act as the stronger electron acceptors through adsorption on the graphitic-like GaN surface.

For calculating the adsorption energy, the total energy of the NO, NO_2, and NH_3 molecules and GaN and GaP surfaces should be computed. As it has been shown in Scheme 1, we have built a graphitic-like of length 25 Å with bond length of 1.95 Å for GaN and 2.28 Å for GaP. Then, we have tailored the spin-polarized DFT calculation with "ONIOM" model [66] accompanying the same force and energy convergence accuracy to the adsorption systems, with CAM-B3LYP [67] functional and with 6–311 + G (d,p) [68] basis set for hydrogen, nitrogen, oxygen, and LANL2DZ for gallium in the adsorption sites for the first layer (high level). Second layer (medium level) has been considered on some gallium atoms and nitrogen or phosphorus atoms of GaN or GaP nanosheets, respectively, in the adsorption site due to semi-empirical methods. The third layer (low level) has been saved on the remained gallium atoms and also remained nitrogen or phosphorus atoms of GaN or GaP nanosheets with molecular mechanic force fields (Scheme 2) [66] as formula: $E_{ONIOM} = E_{1st} + E_{2nd} + E_{3rd}$.

To determine the most sensitive structure of gallium nitride (GaN) and gallium phosphide (GaP) as the selective sensor for detecting gas molecules of NO, NO_2, and NH_3, the binding energy of each system has been calculated. Therefore, we have found that the priority for selecting the surface binding of N-atom of NO, NH_3, and O-atom of NO_2 in adsorption site can be impacted by the existence of close atoms in the GaN and GaP surfaces. The simulated distribution functions of NO → GaN/GaP, NO_2 → GaN/GaP, and NH_3 → GaN/GaP have illustrated that the created clusters

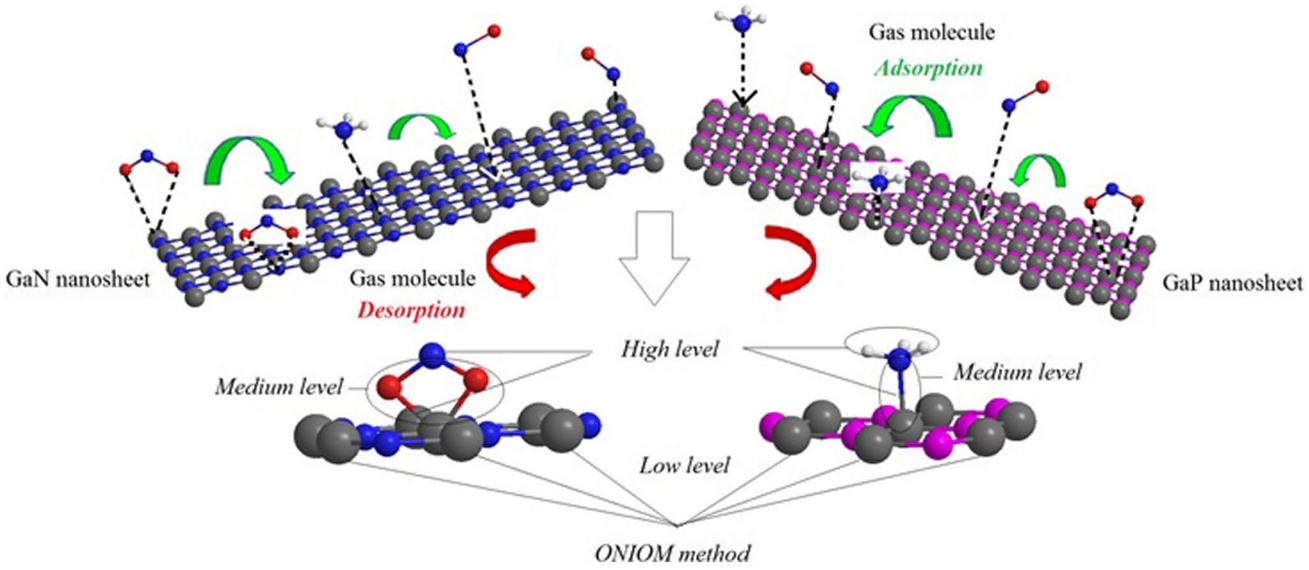

Scheme 2 The mechanism of the "Langmuir" adsorption of NO, NO_2, and NH_3 molecules onto GaN and GaP nanosheets based on optimized coordination due to three-layered of high, medium, and low levels of "ONIOM" method

lead to the bond lengths of N → Ga in NO → GaN/GaP (1.41 Å GaN, 1.44 Å GaP), O → Ga in NO_2 → GaN/GaP (2. 43 Å GaN, 2. 44 Å GaP), and N → Ga in NH_3 → GaN/GaP (2. 19 Å GaN, 2.21 Å GaP) (Schemes 1 and 2).

Results and discussion

In this verdict, gallium nitride (GaN) and gallium phosphide (GaP) nanosheets have been investigated as the efficient surface because of their structural selectivity for adsorption of nitric oxide (NO), nitrogen dioxide (NO_2), and ammonia (NH_3). These experiments have been accomplished using spectroscopy analysis through some physical and chemical properties.

Electronic properties

The electronic structures of NO and NO_2 adsorbed on the GaN and GaP nanosheets have been analyzed to simplify subsequent discussion for interfacial electronic properties using CAM-B3LYP/LANL2DZ, 6–311 + G (d,p) basis sets. The graph of partial DOS (PDOS) has illustrated that the *p* states of the adsorption of N- and O- on the GaN and GaP nanosheets are dominant through the conduction band (Fig. 1). A distinct metallic feature can be observed in GaN and GaP nanosheets because of the strong interaction between the *p* states of N and P and the *d* state of Ga near the Fermi energy. Moreover, the existence of covalent features for these complexes has exhibited the identical energy amount and figure of the PDOS for the *p* orbitals of N, O, and P and *d* orbitals of Ga (Fig. 1).

Figure 1a and a′ show that the NO states in both of GaN and GaP nanosheets, respectively, have more contribution at the middle of the conduction band between − 5 and − 10 eV, while contribution of gallium and phosphorus states are expanded and close together, but nitrogen and oxygen states have minor contributions. In addition, Fig. 1b and b′ illustrate the adsorption of NO_2 onto GaN and GaP nanosheets, respectively, have more contribution at the middle of the conduction band between − 5 and − 10 eV, while contribution of gallium and phosphorus states are expanded and close together, but nitrogen and oxygen states have minor contributions.

The results also approved by the partial electron density (PDOS) which have showed a certain charge association between GaN and GaP nanosheets and gas molecules of NO and NO_2.

In other words, the P states in GaP nanosheet have large contributions in the valence band, while N states in GaN nanosheet have less contribution. Thus, the above results exhibit that the cluster dominant of non-metallic and metallic features and a certain degree of covalent features can illustrate the increasing of the semiconducting direct band gap of gas molecules adsorbing on the GaN and GaP nanosheets.

Nuclear quadrupole resonance (NQR) analysis

NQR method has been carried out for the complexes of NO, NO_2, and NH_3 adsorption on the graphitic-like GaN and GaP

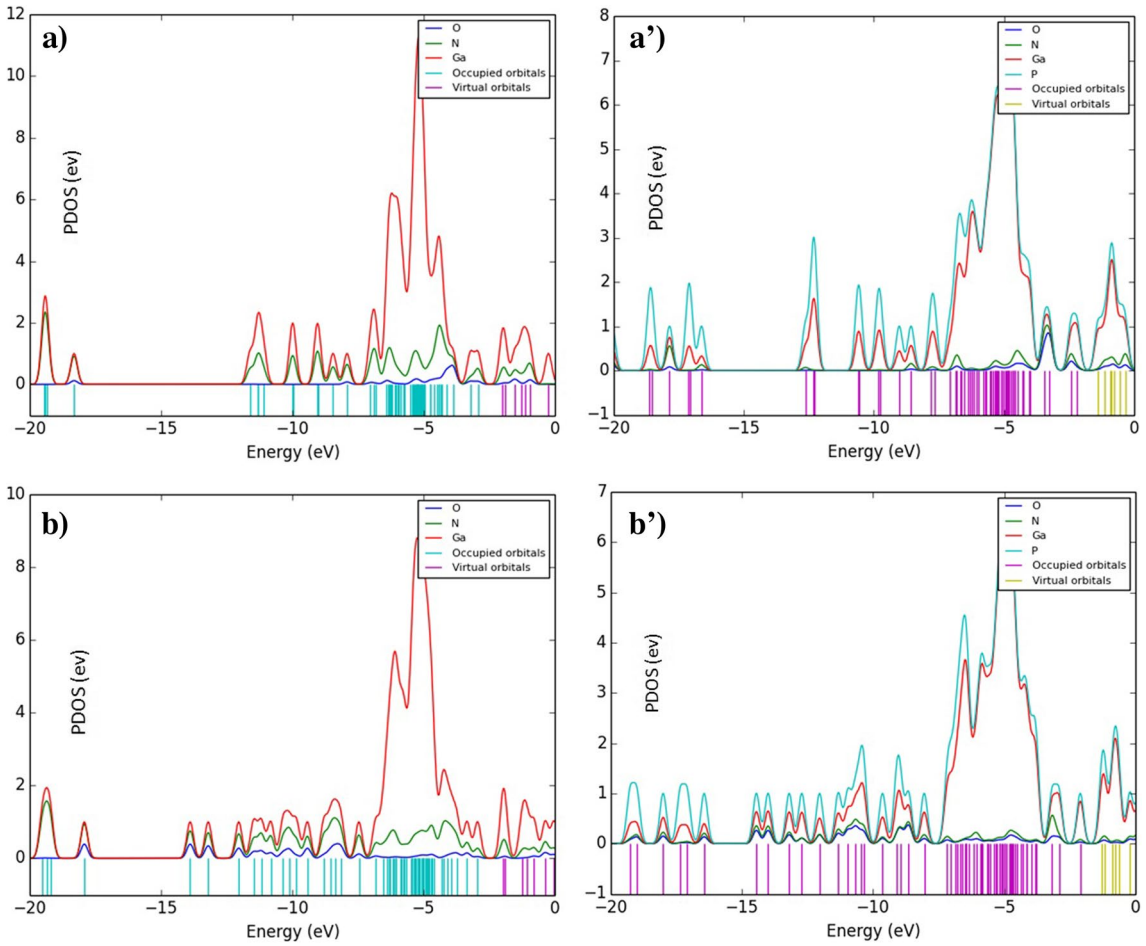

Fig. 1 PDOS adsorption of (**a**) NO → GaN, (**a′**) NO → GaP, (**b**) NO_2 → GaN, and (**b′**) NO_2 → GaP nanosheets with Fermi level = 0

nanosheets. NQR is based on the multipole enlargement in cartesian harmonies as the following equations:

$$V(r) = V(0) + \left[\left(\frac{\partial V}{\partial x_i}\right)\Big|_0 .x_i\right] + \frac{1}{2}\left[\left(\frac{\partial^2 V}{\partial x_i x_j}\right)\Big|_0 .x_i x_j\right] + \ldots \quad (1)$$

Then, after simplification of the equation, there are only the second derivatives dependent on the same variable for the potential energy [69, 70]:

$$U = -\frac{1}{2}\int_{\mathcal{D}} d^3 r \rho_r \left[\left(\frac{\partial^2 V}{\partial x_i^2}\right)\Big|_0 .x_i^2\right] = -\frac{1}{2}\int_{\mathcal{D}} d^3 r \rho_r \left[\left(\frac{\partial E_i}{\partial x_i}\right)\Big|_0 .x_i^2\right] = -\frac{1}{2}\left(\frac{\partial E_i}{\partial x_i}\right)\Big|_0 \cdot \int_{\mathcal{D}} d^3 r\left[\rho(r).x_i^2\right] \quad (2)$$

There are two parameters which must be gotten from NQR experiments: the quadrupole coupling constant, χ, and asymmetry parameter of the EFG tensor η:

$$\chi = {}^{e^2 Q q_{zz}}\Big/_{h} \quad (3)$$

$$\eta = {q_{xx} - q_{yy}}\Big/_{q_{zz}} \quad (4)$$

where q_{ii} are components of the EFG tensor at the quadrupole nucleus determined in the EFG principal axes system; Q is the nuclear quadrupole moment; e is the proton charge, and h is the Planck's constant [71].

The electric potential ($J \cdot C^{-1}$) is a continuous function in space produced by an idealized point charge has 1/r potential: $V_E = \frac{1}{4\pi\varepsilon_0}\frac{Q}{r}$, where Q (measured in coulombs) is the point charge, r is the distance from the charge and ε_0 is the permittivity of vacuum.

Since the electric potential for a system of point charges is equal to the sum of the point charges' individual potentials, the calculations are done simply based on summation of potential fields which is scalar instead of summation of

the electric fields which is vector and much more difficult than potential field. So, $V_E(r) = \frac{1}{4\pi\varepsilon_0}\sum_i \frac{q_i}{|r-r_i|}$, where r is a point at which the potential is measured, r_i is a point at which the charge is $\neq 0$, and q_i is the charge at the point r_i. Finally, the potential of a continuous charge distribution $\rho(r)$ appears: $V_E(r) = \frac{1}{4\pi\varepsilon_0}\int_R \frac{\rho(r')}{|r-r'|}d^3r'$, where R is a region including all the points at which the charge density is $\neq 0$, r' is a point inside R, and $\rho(r')$ is the charge density at the point [72].

As the EFG at the position of the nucleus in gas adsorbed on the gallium nitride and gallium phosphide nanosheets as the gas sensor is assigned by the valence electrons twisted in the special linkage with close nuclei of GaN and GaP nanosurfaces, the NQR frequency at which transitions happen is particular for NO → GaN/GaP, NO_2 → GaN/GaP, and NH_3 → GaN/GaP clusters (Table1).

In addition, in Fig. 2(a–f), it has been plotted the electric potential of NQR method versus Bader charge for elements of hydrogen, nitrogen, phosphorus, oxygen, and gallium in the adsorption process of NO, NO_2, and NH_3 on the GaN and GaP nanosheets using CAM-B3LYP/EPR-III, LANL2DZ, 6–311 + G (d,p) level of theory.

In Fig. 2(a–f), it has been remarked the changes of electric potential for hydrogen, nitrogen, phosphorus, oxygen, and gallium in the active site of Langmuir adsorption. In fact, it has been observed the effect of the binding between H, N, and O with gallium in the GaN and GaP nanosheets

Table 1 The electric potential (E_p) and Bader charge (Q) for elements involving in the adsorption mechanism of NO, NO_2, and NH_3 on the GaN and GaP nanosheets using CAM-B3LYP/EPR-III, 6–311 + G (d,p) calculation extracted of NQR method.

:Ö = Ṅ:→ GaN			:Ö:–Ṅ = Ö:→ GaN			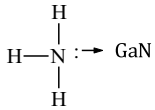		
Atom	Q	E_p	Atom	Q	E_p	Atom	Q	E_p
O1	-0.2246	-22.2691	N1	-0.2230	-18.2043	Ga1	0.2822	-146.59
N2	-0.2626	-18.2995	O2	-0.2686	-22.0279	N2	-0.475	-18.1517
Ga3	0.5194	-147.0664	O3	-0.2213	-21.9945	Ga3	0.2250	-146.608
N4	-0.5262	-18.2340	Ga4	0.34732	-147.21	Ga4	0.2448	-146.605
Ga5	0.4550	-147.089	N5	-0.4432	-18.1789	N5	-0.3370	-18.2079
Ga6	0.4560	-147.0976	Ga6	0.42893	-147.054	Ga6	0.2829	-146.589
N7	-0.4657	-18.2970	Ga7	0.35341	-147.183	N7	-0.3291	-18.1879
Ga8	0.5163	-147.0630	N8	-0.4313	-18.2753	N8	-0.4778	-18.1569
N9	-0.4684	-18.2961	Ga9	0.38506	-147.067	Ga9	0.6245	-146.646
N10	-0.5317	-18.2336	N10	-0.4326	-18.2994	Ga10	0.2323	-146.608
Ga11	0.5978	-147.2992	N11	-0.5487	-18.2298	N11	-0.4627	-18.1606
Ga12	0.4672	-147.0987	Ga12	0.9045	-147.234	Ga12	0.1992	-146.611
N13	-0.5280	-18.2393	Ga13	0.5788	-147.098	N13	-0.3379	-18.2106
Ga14	0.4607	-147.0861	N14	-0.4801	-18.1804	N14	-0.4815	-17.8981
N15	-0.4652	-18.2971	Ga15	0.5136	-147.016	H15	0.2739	-0.89106
			N16	-0.4626	-18.282	H16	0.2685	-0.89209
						H17	0.2676	-0.89065
:Ö = Ṅ:→ GaP			:Ö:–Ṅ = Ö:→ GaP			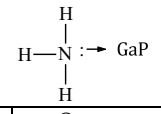		
Atom	Q	E_p	Atom	Q	E_p	Atom	Q	E_p
O1	-0.1121	-22.0983	N1	-0.1672	-18.1325	Ga1	-0.1285	-146.762
N2	-0.1830	-18.1953	O2	-0.2476	-21.9465	P2	0.0143	-53.3774
Ga3	-0.0542	-146.7837	O3	-0.2252	-21.9584	Ga3	-0.0753	-146.745
P4	0.0766	-53.3514	Ga4	-0.0473	-146.824	Ga4	-0.114	-146.758
Ga5	-0.0238	-146.8043	P5	0.1540	-53.306	P5	0.0757	-53.4317
Ga6	-0.0337	-146.7962	Ga6	-0.1367	-146.787	Ga6	-0.1142	-146.735
P7	0.0826	-53.4215	Ga7	-0.1310	-146.787	P7	0.0736	-53.4367
Ga8	-0.0458	-146.7722	P8	0.1304	-53.4033	P8	0.0142	-53.3812
P9	0.1161	-53.4000	Ga9	-0.0419	-146.777	Ga9	0.0728	-146.808
P10	0.0872	-53.3442	P10	0.0977	-53.4119	Ga10	-0.0683	-146.752
Ga11	0.0255	-146.7736	P11	0.0535	-53.3514	P11	0.0086	-53.3811
Ga12	-0.0543	-146.7907	Ga12	0.3515	-146.765	Ga12	-0.1114	-146.765
P13	0.0681	-53.3499	Ga13	-0.0214	-146.816	P13	0.0671	-53.4423
Ga14	-0.0469	-146.7863	P14	0.1766	-53.2955	N14	-0.4618	-17.9438
P15	0.0977	-53.4117	Ga15	-0.0405	-146.766	H15	0.2514	-0.9245
			P16	0.0951	-53.4106	H16	0.2464	-0.9282
						H17	0.2495	-0.9244

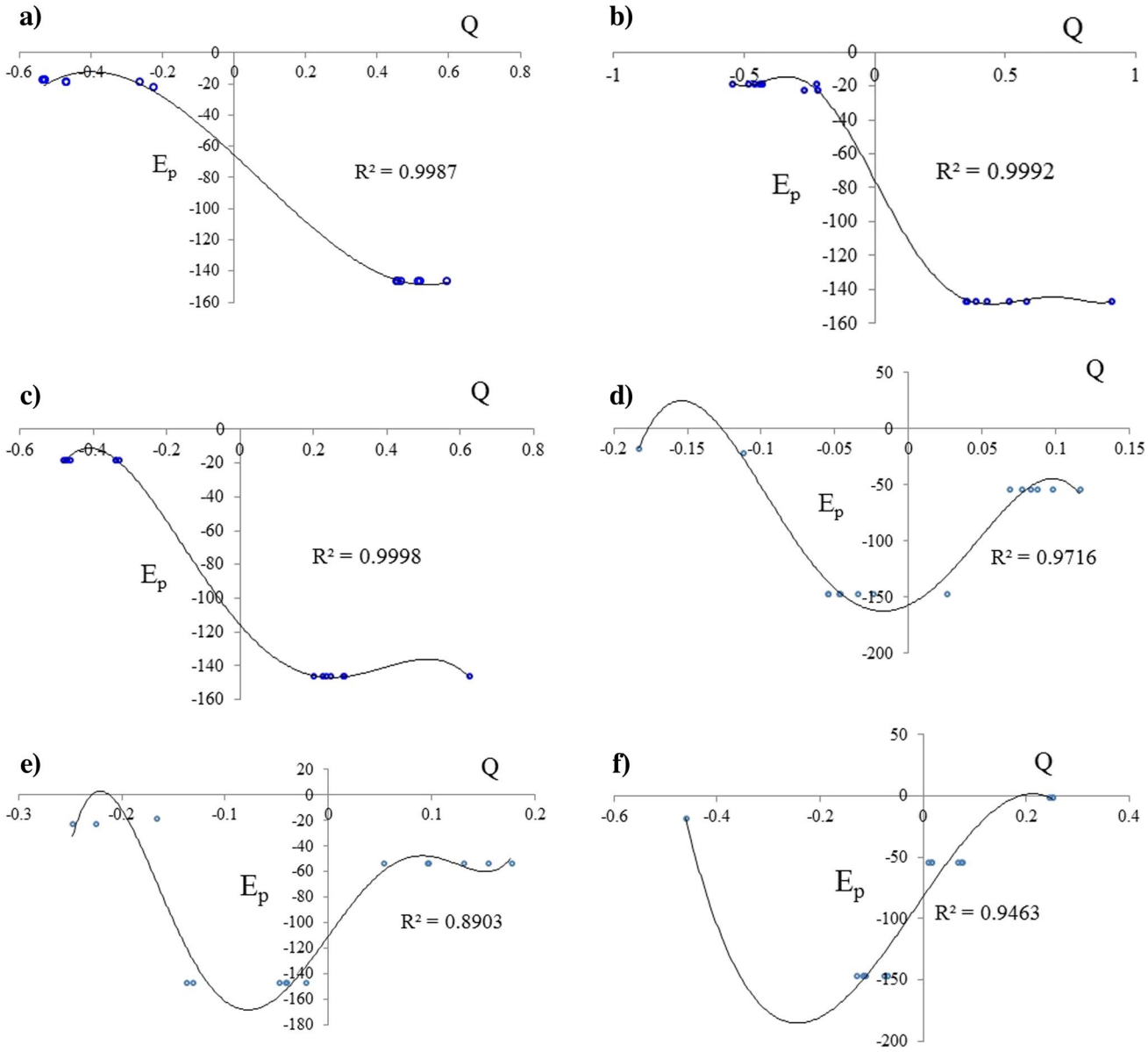

Fig. 2 The electric potential versus Bader charge through NQR calculation for adsorption clusters of (**a**) NO→GaN, (**b**) NO_2→GaN, (**c**) NH_3→GaN, (**d**) NO→GaP, (**e**) NO_2→GaP, (**f**) NH_3→GaP using CAM-B3LYP/EPR-III, LANL2DZ,6–31 + G(d,p)

during adsorbing NO, NO_2, and NH_3 through resulted electric potential using NQR analysis (Fig. 2a–f). It is obvious that the capability of GaN and GaP for detecting of NO, NO_2, and NH_3 is fluctuated by their selectivity and sensitivity which can represent the efficiency of these surfaces as the promising sensors. Furthermore, the GaP surface has indicated a large distribution area for electric potential versus atomic charge compared to GaN surface through gas adsorption (Fig. 2a–f).

"NMR" spectroscopy

Isotropic (σ_{iso}) and anisotropy (σ_{aniso}) shielding tensors of "NMR" spectroscopy for certain atoms in the active site of NO, NO_2, and NH_3 adsorbed on the GaN and GaP nanosheets through the formation of the binding between gas molecules and solid surfaces have been calculated using Gaussian 16, Revision C.01 and reported in Table2 [57].

Table 2 Data of "NMR" shielding tensors for selected atoms of NO, NO_2, and NH_3 through adsorption on GaN and GaP nanosheets using CAM-B3LYP/EPR-III, 6–311 + G (d,p) calculation.

:Ö = Ṅ:→ GaN			:Ö:–Ṅ = Ö:→ GaN			H—N :→ GaN		
Atom	σ iso	σ aniso	Atom	σ iso	σ aniso	Atom	σ iso	σ aniso
O1	4821.8747	13220.5719	N1	830.2777	6372.8449	Ga1	17626.0171	29573.0338
N2	737.8156	6496.7109	O2	1323.1030	6727.1193	N2	251.8641	354.4383
Ga3	2451.1239	29825.8262	O3	388.6740	3388.9901	Ga3	20005.1261	34085.0813
N4	1469.7502	3402.7758	Ga4	30814.9219	58182.6146	Ga4	17897.4195	29633.6318
Ga5	15553.2422	25607.9058	N5	1442.7706	13067.9649	N5	175.9060	629.9592
Ga6	11515.0022	20178.1529	Ga6	4010.8252	49917.8649	Ga6	17239.2677	29092.0179
N7	4314.9928	14492.9754	Ga7	26441.6944	114676.7699	N7	187.6651	394.6117
Ga8	2696.7458	37790.2395	N8	2338.2041	36057.6300	N8	232.8229	258.9451
N9	775.1003	2658.5011	Ga9	7173.4867	80927.3080	Ga9	16327.1187	23810.0447
N10	741.1297	3607.7969	N10	3879.4503	45938.3647	Ga10	18576.5314	30716.4928
Ga11	109.3018	2065.2926	N11	950.1517	4548.8274	N11	234.2999	503.8588
Ga12	3361.2055	10569.2187	Ga12	1439.0401	3651.1223	Ga12	19557.5661	33305.4682
N13	1448.2707	3249.5646	Ga13	18631.5643	74813.8800	N13	129.2701	618.9554
Ga14	7061.5546	16864.5428	N14	887.1812	9987.7736	N14	295.8192	25.3839
N15	150.5372	3369.7321	Ga15	15303.0265	23988.9456	H15	34.4223	13.4819
			N16	159.5638	5975.1969	H16	37.1167	14.4223
						H17	37.8487	18.8085
:Ö = Ṅ:→ GaP			:Ö:–Ṅ = Ö:→ GaP			H—N :→ GaP		
Atom	σ iso	σ aniso	Atom	σ iso	σ aniso	Atom	σ iso	σ aniso
O1	4291.3737	18144.2304	N1	963.1386	5073.9512	Ga1	9857.8109	15414.6899
N2	1501.5049	7351.6689	O2	449.7992	1347.3262	P2	767.7419	379.4713
Ga3	11101.4880	32961.8880	O3	240.2882	1770.9646	Ga3	7177.7779	12159.4075
P4	1345.6299	2994.8451	Ga4	250.7804	17847.5451	Ga4	8870.3588	14309.8508
Ga5	4597.8176	13217.0292	P5	7.4632	2349.9993	P5	175.9657	1025.7263
Ga6	8863.2663	27092.9349	Ga6	2265.7391	35940.7712	Ga6	8447.8970	14438.1778
P7	2450.3875	8540.9915	Ga7	1778.5600	16061.2490	P7	128.2753	923.3844
Ga8	10528.6575	42599.5393	P8	1540.9587	6540.2528	P8	740.2248	316.9980
P9	2005.8726	12528.0484	Ga9	5545.2324	30081.3134	Ga9	725.8970	320.3635
P10	2001.5489	5508.0432	P10	1832.7918	10443.3200	Ga10	6267.2422	10271.4430
Ga11	74.6069	7545.0632	P11	1214.9676	2235.8903	P11	753.2626	173.0349
Ga12	2070.4614	10425.6100	Ga12	2046.9346	2697.7003	Ga12	9525.8790	13366.4292
P13	1077.9593	1502.2900	Ga13	280.8469	10404.0217	P13	113.3957	1260.7633
Ga14	12773.7755	21777.8000	P14	581.4133	946.6701	N14	251.9207	60.8834
P15	786.8145	4011.5859	Ga15	12061.3717	22237.3411	H15	32.1285	14.8191
			P16	2577.7451	6181.6267	H16	30.9170	14.8849
						H17	31.4410	14.3654

"Isotropic chemical-shielding" (σ_{iso}) and "anisotropic chemical-shielding" (σ_{aniso}) [73]: $\sigma_{iso} .= \frac{\sigma 33+\sigma 22+\sigma 11}{3} \sigma_{aniso} = \sigma 33 - \frac{\sigma 22+\sigma 11}{2}$

It was observed the chemical shielding (ppm) of "NMR" curves versus atom type through adsorption of NO, NO_2, and NH_3 onto GaN and GaP nanosheets (Fig. 3).

The resulted graphs of "NMR" data in Fig. 3(a–c, a′–c′) have shown approximately the identical chemical shielding behavior of isotropic and anisotropy factors for NO → GaN/GaP nanosheets with several sharp peaks related to gallium atoms involving the adsorption site (Ga3, Ga5, Ga6, Ga8, Ga12, Ga14) (Fig. 3a, a′), NO_2 → GaN/GaP nanosheets with several sharp peaks related to gallium atoms involving the adsorption site (Ga4, Ga6, Ga7, Ga9, Ga13, Ga15) (Fig. 3b, b′), and NH_3 → GaN/GaP nanosheets with several sharp peaks related to gallium atoms corresponding the adsorption site (Ga1, Ga3, Ga4, Ga6, Ga10, Ga12) (Fig. 3c, c′). Although, in the NMR spectroscopy, it has been observed the remarkable peak around gallium atom in the GaN and GaP nanosheets through the adsorption procedure of gas molecules, there are some fluctuations in the chemical shielding behaviors of isotropic and anisotropy attributes. Moreover, Fig. 3(a–c, a′–c′) has exhibited that the magnetic gap between chemical shielding of isotropic and

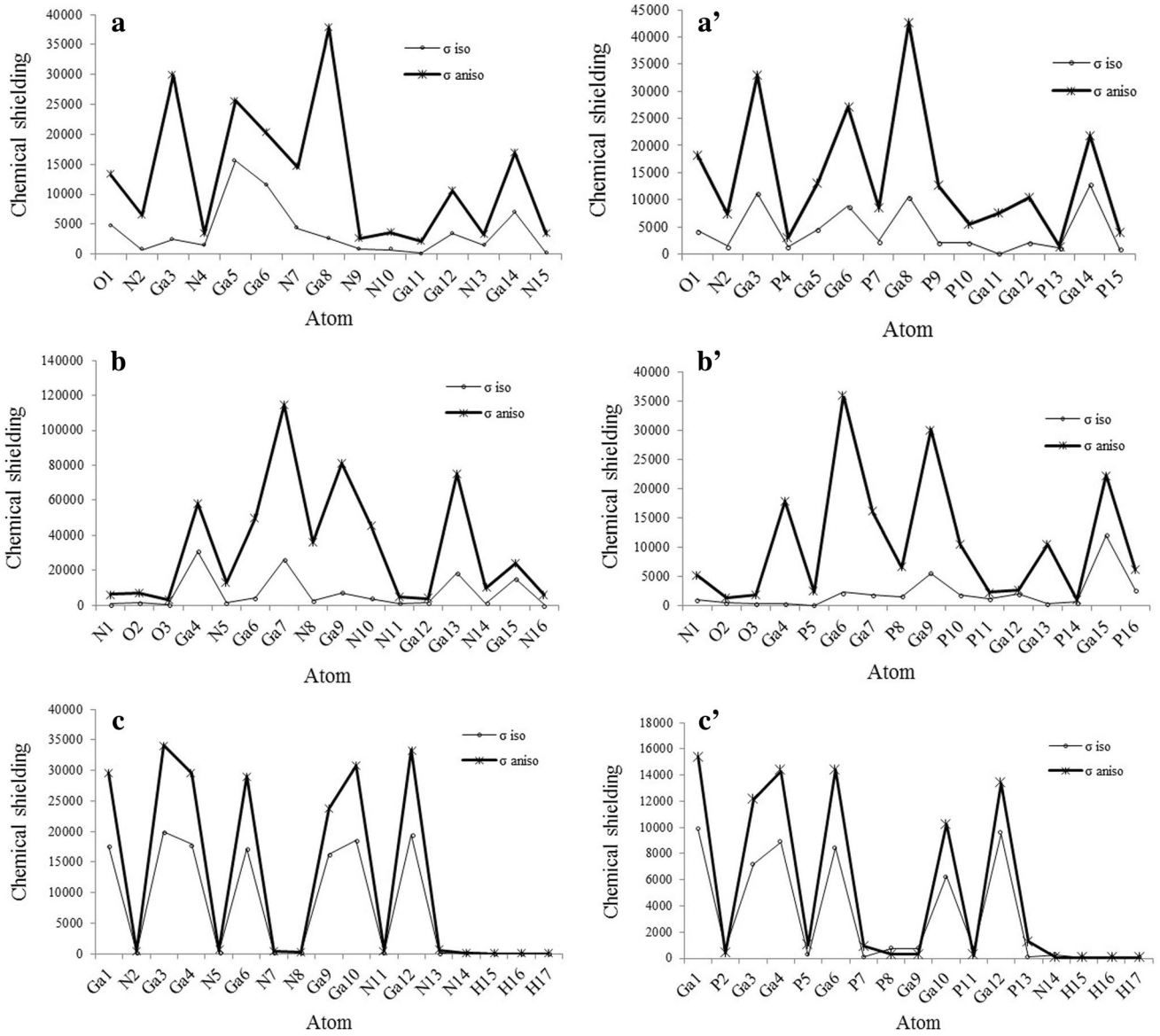

Fig. 3 "NMR" adsorbing of NO, NO_2, NH_3 on the GaN, and GaP nanosheets through production of clusters of (**a**) NO → GaN, (**a′**) NO → GaP, (**b**) NO_2 → GaN, (**b′**) NO_2 → GaP, (**c**) NH_3 → GaN, and (**c′**) NH_3 → GaP

anisotropy for the GaN surface through gas adsorption is larger than this parameter for the GaP surface.

"IR" insight and thermodynamic analysis

In this part, the stability of complexes including gas adsorption on graphitic gallium nitride (GaN) and graphitic gallium phosphide (GaP) has been investigated through thermodynamic properties which define the reactions that gas molecules of nitric oxide (NO), nitrogen dioxide (NO_2), and ammonia (NH_3) endure in the gallium coordination sphere. Concerning adsorption process, the thermodynamic characters were evaluated for NO, NO_2, and NH_3 on the surfaces of graphitic gallium nitride (GaN) and graphitic gallium phosphide (GaP) as the gas detectors which can be applicable as the selective sensors for these gases (Table 3).

Furthermore, the "IR" spectrums for adsorption of NO, NO_2, and NH_3 on the surfaces of GaN and GaP nanosheets have been reported in Fig. 4.

The graphs of Fig. 4(a, a′) have been observed in the frequency range between 50 and 500 cm^{-1} for the complexes of NO → GaN and NO → GaP, respectively, with a sharp peak around 200 cm^{-1}.

Figure 4 (b, b′) has shown the several strongest IR peaks of NO_2 → GaN and NO_2 → GaP clusters approximately between 200 and 1150 cm^{-1}. Besides, it has been

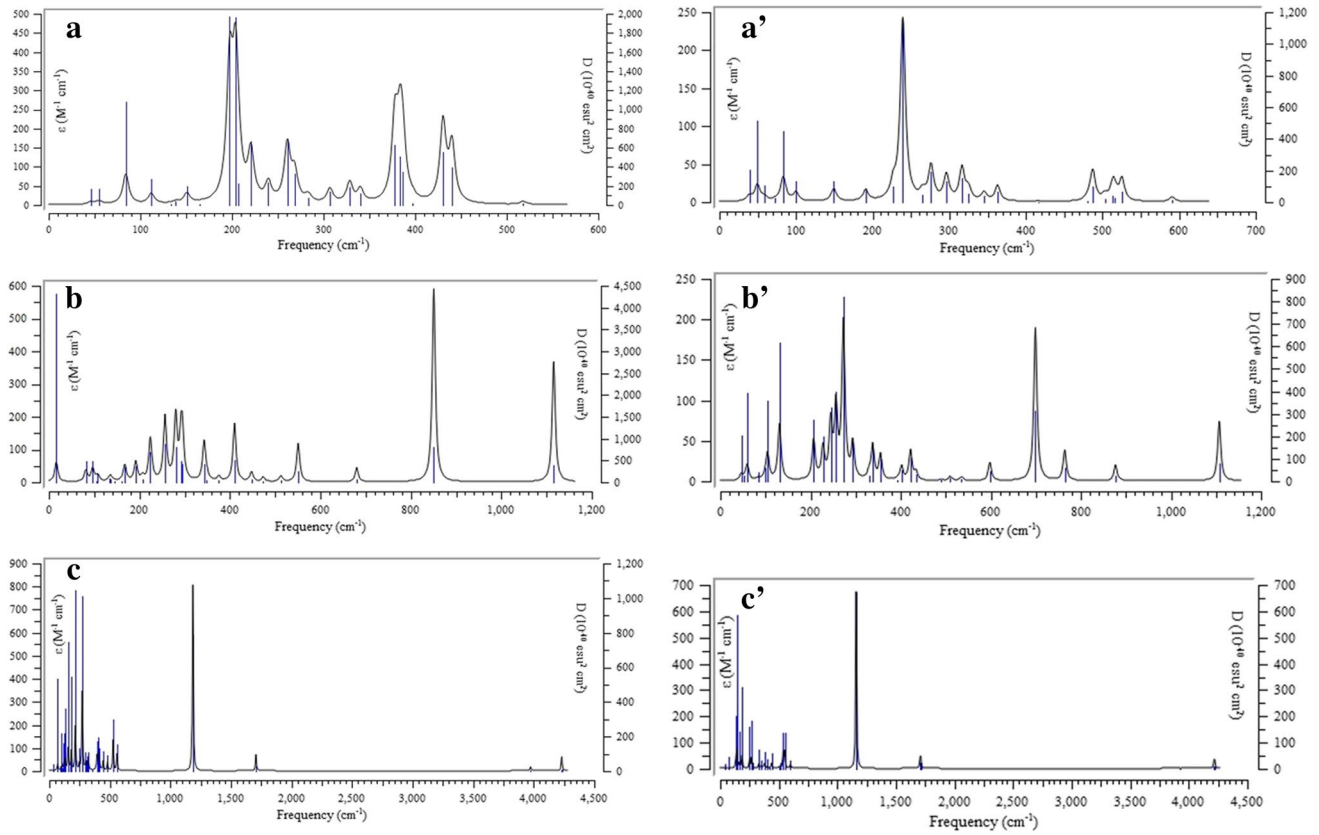

Fig. 4 The frequency (cm^{-1}) changes through the "IR" spectrums for (**a**) NO → GaN, (**a′**) NO → GaP, (**b**) NO_2 → GaN, (**b′**) NO_2 → GaP, (**c**) NH_3 → GaN, and (**c′**) NH_3 → GaP nanosheets as the selective gas detectors

seen the frequency sharp peaks of 850 cm^{-1}, 1150 cm^{-1} for NO_2 → GaN and 265 cm^{-1}, 700 cm^{-1} for NO_2 → GaP, respectively (Fig. 4b, b′). Furthermore, the several strong frequency fluctuations for NH_3 → GaN and NH_3 → GaP nanosheets have been represented between 100 and 1200 cm^{-1} with a sharp peak around 1150 cm^{-1} for both NH_3 → GaN and NH_3 → GaP complexes (Fig. 4c, c′).

In addition, the high amounts of the "Langmuir" adsorption isotherm graphs based on relative adsorption energy (ΔE°_{ads}) have been evaluated for interactions between NO, NO_2, and NH_3 on the surfaces of GaN and GaP nanosheets with $R^2 = 0.9062$ (Fig. 5). The order of ΔE°_{ads} for gas molecules adsorption on GaP nanosheet has indicated more stability compared to relative energy changes of gas molecules adsorption on GaN nanosheet (Fig. 5).

The adsorptive capacity of NO, NO_2, and NH_3 on the surfaces of GaN and GaP is approved by the ΔE°_{ads} amounts as formula:

$\Delta E^{\circ}_{ads} = \Delta E^{\circ}_{X\rightarrow GaN/GaP} - (\Delta E^{\circ}_{X} + \Delta E^{\circ}_{GaN/GaP})$; ($X$ = NO, NO_2, NH_3).

Table 3 has shown that the adsorbing of NO, NO_2, and NH_3 on the surfaces of GaN and GaP nanosheets must have both "physical" and "chemical" nature. All the measured relative adsorption energies (ΔE°_{ads}) are almost identical, and exhibit the accord of the estimated data by all methods and the accuracy of the calculations (Fig. 5). In fact, Ga sites in GaN and GaP nanosheets have higher interaction energy from Van der Waals' forces with gas molecules including NO, NO_2, and NH_3 that can make them highly stable.

Furthermore, the results of Table 3 have indicated that NO → GaP, NO_2 → GaP, NH_3 → GaP nanosheets have the largest gap of Gibbs free energy adsorption with which defines the changes between Gibbs free energy of initial compounds (ΔG°_{NO}, ΔG°_{NO2}, ΔG°_{NH3}), and (ΔG°_{GaP}) and product compounds ($\Delta G^{\circ}_{NO\rightarrow GaP}$, $\Delta G^{\circ}_{NO2\rightarrow GaP}$, $\Delta G^{\circ}_{NH3\rightarrow GaP}$) through polarizability. However, GaN and GaP nanosheets seem to possess enough efficiency for adsorption toxic gases of NO, NO_2, and NH_3 through charge transfer from nitrogen and oxygen to the gallium element due to intra-atomic and interatomic interactions.

Analysis of "HOMO, LUMO"

Based on frontier molecular orbital "FMO" theory, the "LUMO" and "HOMO" and the energy between them is the band gap of the adsorption system were computed. In

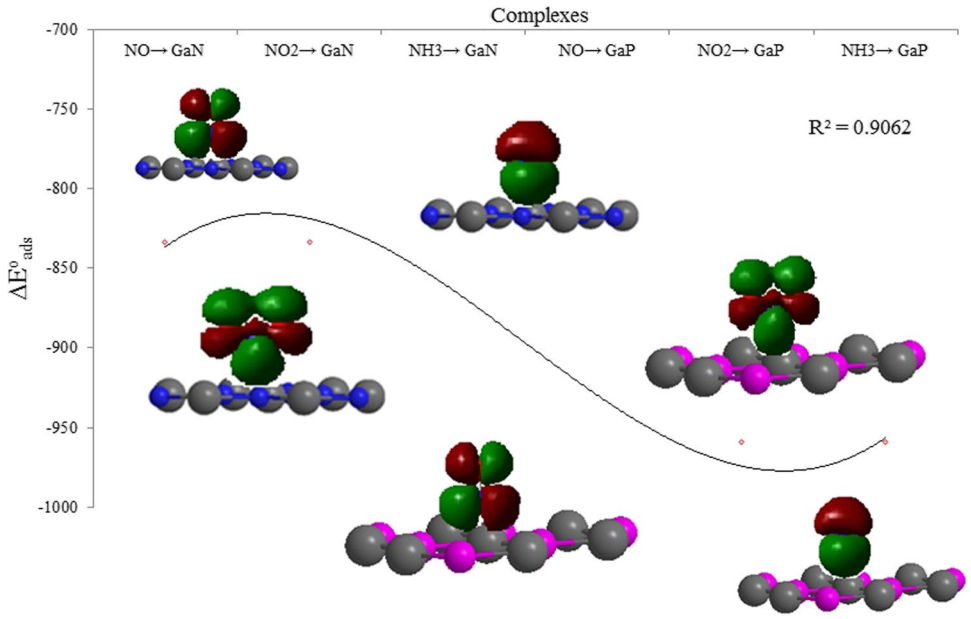

Fig. 5 The alterations of relative adsorption energy (ΔE°_{ads}) for NO, NO_2, and NH_3 adsorbed on the surfaces of GaN and GaP nanosheets

fact, broad band gap diagram indicates that there is less conductivity [74–76]. The "LUMO," "HOMO," band energy gap (ΔE), and other quantity distributions of NO, NO_2, and NH_3 on the surfaces of GaN and GaP nanosheets as the gas detector systems denote that the gas adsorption procedure scatters the electrons of the system (Table 4).

The energy gap between HOMO and LUMO has represented the transporting of molecular electrical characters [77]. On the other hand, the difference between HOMO and LUMO has exhibited that the effect of the adsorption process on the electronic behavior of NO, NO_2, and NH_3 on the surfaces of GaN and GaP nanosheets (Table 4). "μ" which shows chemical potential accompanying negative worth using B3LYP/ LANL2DZ, 6–311 + G (d, p), has an agreeable yield for capturing NO, NO_2, and NH_3 by GaN and GaP nanosheets (Table 4).

The illustration of donor–acceptor molecules depends on the relative frontier molecular levels. The HOMO–LUMO gap defines the charge transfer in gas molecules adsorbed on the GaN and GaP surfaces through simplified molecular-level diagram. In fact, the amount of transferred charges might be considerably small, as in the case of parallel and perpendicular coordination, which indicate electronic couplings smaller than in co-facial coordination. The results in Table 4 have indicated the energy level shifts of gas molecule → surface-HOMO and gas molecule → surface -LUMO of nanoclusters as a function of their distance *d* orbitals from the high symmetry points of each gas molecule on the GaN and GaP surfaces. Therefore, the HOMO level of molecule is being lowered as it loses its electron, whereas the LUMO level of surface is being raised as it gains partial charge.

Table 3 The thermodynamic character of NO, NO_2, and NH_3 adsorbed on the GaN and GaP nanosheets as the selective gas sensors

Compound	$\Delta E^{\circ} \times 10^{-4}$ (kcal/mol)	$\Delta E^{\circ}_{ads} \times 10^{-4}$ (kcal/mol)	$\Delta H^{\circ} \times 10^{-4}$ (kcal/mol)	$\Delta G^{\circ} \times 10^{-4}$ (kcal/mol)	S° (Cal/K.mol)	Dipole moment (Debye)
Ga-N	−21.4958	-	−21.4957	−21.4998	137.460	0.6307
Ga-P	−3.2937	-	−3.2936	−3.2964	91.515	0.4347
NO	−8.0017	-	−8.0016	−8.0031	48.968	0.2376
NO_2	−12.6298	-	−12.6298	−12.6315	57.792	0.2323
NH_3	−3.5437	-	−3.5436	−3.5450	48.176	2.1281
NO → GaN	−863.1604	−833.6629	−863.1604	−863.1644	133.724	4.8379
NO_2 → GaN	−867.7891	−833.6635	−867.7890	−867.7931	135.598	4.4976
NH_3 → GaN	−859.3971	−834.3576	−859.3970	−859.4014	145.511	5.0153
NO → GaP	−970.6414	−959.3460	−970.6413	−970.6453	131.438	2.3266
NO_2 → GaP	−975.2858	−959.3623	−975.2858	−975.2897	130.628	2.0852
NH_3 → GaP	−966.1167	−959.2793	−966.1167	−966.1202	117.609	4.4479

Table 4 "LUMO" (a.u.), "HOMO" (a.u.), band energy gap (ΔE/ev), and other quantity (ev) distributions of NO, NO_2, and NH_3 adsorbed on the surfaces of GaN and GaP nanosheets.

Gas→ GaN/GaP	LUMO	HOMO	ΔE	μ	χ	η	ζ	ψ
NO→GaN	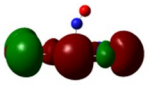 0.0447	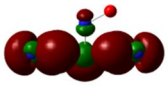 -0.0868	3.5783	-0.5733	0.5733	1.7891	0.2794	0.3888
NO_2→GaN	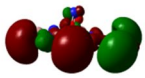 0.0257	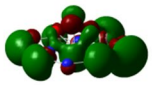 -0.1157	3.8496	-1.2235	1.2235	1.9248	0.2597	0.0918
NH_3→GaN	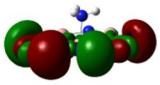 -0.0658	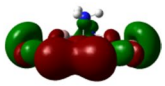 -0.1486	2.2552	-2.9176	2.9176	1.1276	0.4434	3.7745
NO→GaP	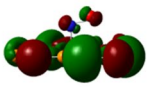 -0.0512	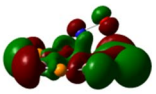 -0.0803	0.7910	-1.7893	1.7893	0.3955	1.2642	4.0475
NO_2→GaP	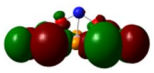 -0.0469	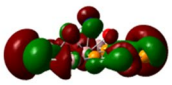 -0.0771	0.8212	-1.6871	1.6871	0.4106	1.2177	3.4660
NH_3→GaP	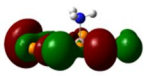 -0.0352	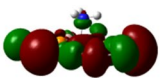 -0.0983	1.7156	-1.8165	1.815	0.8578	0.5829	1.9233

Band energy gap: $\Delta E = E_{LUMO} - E_{HOMO}$; Chemical potential: $\mu = (E_{HOMO} + E_{LUMO})/2$; Electronegativity: $\chi = -(E_{HOMO} + E_{LUMO})/2$; Hardness: $\eta = (E_{LUMO} - E_{HOMO})/2$; Softness: $\zeta = 1/(2\eta)$; electrophilicity index: $\psi = \mu^2/(2\eta)$ [74–76].

Conclusion

The current research wanted to remark the illustration of gas adsorption on GaN and GaP nanosheets. Particularly, the structural, energetic, and infrared adsorption properties of linearly "atop" for NO, NO_2, and NH_3 molecules adsorbing on GaN and GaP nanosheets have been explored by using DFT calculations.

The values of changes of charge density have shown a more important charge transfer for GaN compared to GaP which acts both as the electron donor while gas molecules act as the stronger electron acceptors through adsorption on the graphitic-like GaN surface. It has been assumed that the priority for selecting the surface binding of N-atom of NO, NH_3, and O-atom of NO_2 in adsorption site can be impacted by the existence of close atoms in the GaN and GaP surfaces.

In fact, Ga sites in GaN and GaP nanosheets have higher interaction energy from Van der Waals' forces with gas molecules including NO, NO_2, and NH_3 that can make them highly stable. Finally, our molecular simulation consequences have exhibited the existence of orbital hybridization between gallium sites and gas molecules of NO, NO_2, and NH_3 that also approves the recovery of adsorption susceptibility of graphene sheet. In fact, GaN and GaP nanosheets can promise an applicable outlook in the field of NO, NO_2, and NH_3 gas sensor.

Acknowledgements In successfully completing this paper and its research, the authors are grateful to Kastamonu University for their support through the office, library, and scientific websites.

Author contribution Fatemeh Mollaamin: conceptualization and idea, methodology, software, validation, formal analysis, investigation, data curation, writing—original draft preparation, visualization, supervision, project administration.

Majid Monajjemi: methodology, software, formal analysis, investigation, data curation, writing—review and editing, visualization, resources.

Data availability It is not applicable.

Declarations

Ethical approval The authors consent to participate and publish the data.

Competing interests The authors declare no competing interests.

References

1. Kroto HW, Heath JR, O'Brien SC, Curl RF, Smalley RE (1985) C60: Buckminsterfullerene. Nature 318:162–163
2. Nasibulin AG, Pikhitsa PV, Jiang H, Brown DP, Krasheninnikov AV, Anisimov AS, Queipo P, Moisala A, Gonzalez D, Lientschnig G et al (2007) A Novel Hybrid Carbon Material. Nat Nanotechnol 2:156–161
3. Moisala A, Nasibulin AG, Shandakov SD, Jiang H, Kauppinen EI (2005) On-Line Detection of single-walled carbon nanotube formation during aerosol synthesis methods. Carbon 43:2066–2074
4. Mollaamin F, Monajjemi M (2023) Doping of graphene nanostructure with iron, nickel and zinc as selective detector for the toxic gas removal: a density functional theory study. C 9:20. https://doi.org/10.3390/c9010020.
5. Schedin F, Geim AK, Morozov SV, Hill EW, Blake P, Katsnelson MI, Novoselov KS (2007) Nat Mater 6:652–655
6. He Q, Wu S, Yina Z, Zhang H (2012) Chem Sci 3:1764–1772
7. Monajjemi M, Khaleghian M, Tadayonpour N, Mollaamin F (2010) The effect of different solvents and temperatures on stability of single-walled carbon nanotube: a QM/MD study. Int J Nanosci 09:517–529. https://doi.org/10.1142/S0219581X10007071
8. Mollaamin F, Ilkhani A, Sakhaei N, Bonsakhteh B, Faridchehr A, Tohidi S, Monajjemi M (2015) Thermodynamic and solvent effect on dynamic structures of nano bilayer-cell membrane: hydrogen bonding study. J Comput Theor Nanosci 12:3148–3154. https://doi.org/10.1166/jctn.2015.4092
9. Khalili Hadad B, Mollaamin F, Monajjemi M (2011) Biophysical chemistry of macrocycles for drug delivery: a theoretical study. Russ Chem Bull 60:238–241. https://doi.org/10.1007/s11172-011-0039-5
10. Su Y, Wang J, Wang B, Yang T, Yang B, Xie G, Zhou Y, Zhang S, Tai H, Cai Z et al (2020) Alveolus-inspired active membrane sensors for self-powered wearable chemical sensing and breath analysis. ACS Nano 14:6067–6075. https://doi.org/10.1021/acsnano.0c01804
11. Ma D, Zhang J, Li X, He C, Lu Z, Lu Z, Lu Z, Yang Z, Wang Y (2018) C3N monolayers as promising candidates for NO_2 sensors. Sens Actuators B Chem 266:664–673. https://doi.org/10.1016/j.snb.2018.03.159
12. Mollaamin F (2014) On the behavior of boron nitride nanotube-flavin adenine dinucleotide interaction ion implantation order to design biofuel cells. J Comput Theor Nanosci 11(9):2017–2022
13. Tahan A, Mollaamin F, Monajjemi M (2009) Thermochemistry and NBO analysis of peptide bond: investigation of basis sets and binding energy. Russ J Phys Chem A 83:587–597. https://doi.org/10.1134/S003602440904013X
14. Monajjemi M, Baie MT, Mollaamin F (2010) Interaction between threonine and cadmium cation in [Cd(Thr)] (n = 1–3) complexes: density functional calculations. Russ Chem Bull 59:886–889. https://doi.org/10.1007/s11172-010-0181-5
15. Zadeh MA (2015) Akbari; Lari, Hadi; Kharghanian, Leyla; Balali, Ebrahim; Khadivi, Ramona; Yahyaei, Hooriye; Mollaamin, Fatemeh; Monajjemi, Majid, Density functional theory study and anti-cancer properties of shyshaq plant: in view point of nano biotechnology. J Comput Theor Nanosci 12:4358–4367. https://doi.org/10.1166/jctn.2015.4366
16. Mollaamin F, Monajjemi M, Salemi S, Baei MT (2011) A dielectric effect on normal mode analysis and symmetry of BNNT Nanotube. Fuller Nanotub Carbon Nanostructures 19:182–196. https://doi.org/10.1080/15363831003782932
17. Lee SW, Lee W, Hong Y, Lee G, Yoon DS (2018) Recent advances in carbon material-based NO2 gas sensors. Sens Actuators B Chem 255:1788–1804. https://doi.org/10.1016/j.snb.2017.08.203
18. Mollaamin F, Monajjemi M (2023) Corrosion inhibiting by some organic heterocyclic inhibitors through Langmuir adsorption mechanism on the Al-X (X = Mg/Ga/Si) alloy surface: a study of quantum three-layer method of CAM-DFT/ONIOM. J Bio Tribo Corros 9:33. https://doi.org/10.1007/s40735-023-00751-y
19. Xiao Z, Kong LB, Ruan S, Li X, Yu S, Li X, Jiang Y, Yao Z, Ye S, Wang C et al (2018) Recent development in nanocarbon materials for gas sensor applications. Sens Actuators B Chem 274:235–267. https://doi.org/10.1016/j.snb.2018.07.040
20. Khan MAH, Rao MV, Li Q (2019) Recent advances in electrochemical sensors for detecting toxic gases: NO2, SO2 and H2S. Sensors 19:905. https://doi.org/10.3390/s19040905
21. Bakhshi K, Mollaamin F, Monajjemi M (2011) Exchange and correlation effect of hydrogen chemisorption on nano V(100) surface: a DFT study by generalized gradient approximation (GGA). J Comput Theor Nanosci 8:763–768. https://doi.org/10.1166/jctn.2011.1750
22. Mahdavian L, Monajjemi M (2010) Alcohol sensors based on SWNT as chemical sensors: Monte Carlo and Langevin dynamics simulation. Microelectron J 41:142–149. https://doi.org/10.1016/j.mejo.2010.01.011
23. Johansson JKE, Mellqvist J, Samuelsson J, Offerle B, Lefer B, Rappenglück B, Flynn J, Yarwood G (2014) Emission measurements of alkenes, alkanes, SO2, and NO2 from stationary sources in Southeast Texas over a 5 year period using SOF and mobile DOAS. J Geophys Res Atmos 119:1973–1991. https://doi.org/10.1002/2013JD020485
24. Clark T, Murray JS, Politzer P (2018) A perspective on quantum mechanics and chemical concepts in describing noncovalent interactions. Phys Chem Chem Phys 20(48):30076–30082. https://doi.org/10.1039/C8CP06786D
25. Cui S, Pu H, Wells SA, Wen Z, Mao S, Chang J, Hersam MC, Chen J (2015) Nat Commun 6:8632
26. Batmunkh M, Bat-Erdene M, Shapter JG (2016) Adv Mater 28:8586–8617
27. Hussain T, Kaewmaraya T, Chakraborty S, Ahuja R (2016) J Phys Chem C 120:25256–25262
28. Chandramouli R, Srivastava A, Nagarjan V (2015) Appl Surf Sci 351:662–672
29. Duan X, Lieber CM (2000) General synthesis of compound semiconductor nanowires. Adv Mater 12:298–302
30. Owens A, Peacock A (2004) Compound semiconductor radiation detectors. Nucl Instrum Methods Phys Res Sect A Accel Spectrometers Detect Assoc Equip 531:18–37
31. Ikawa Y, Lee K, Ao J-P, Ohno Y (2014) Two-dimensional device simulation of AlGaN/GaN heterojunction FET side-gating effect. Jpn J Appl Phys 53:114302
32. Podolska A, Seeber RM, Mishra UK, Pfleger KDG, Parish G, Nener BD (2012) Detection of biological reactions by AlGaN/GaN biosensor. In Proceedings of the COMMAD 2012, Melbourne, Australia, 12–14 December 2012; pp. 75–76.
33. Prokopuk N, Son K-A, George T, Moon JS (2005) Development of GaN-based micro chemical sensor nodes. In Proceedings of the IEEE Sensors 2005, Irvine, CA, USA, 30 October–3 November 2005; pp. 199–202.
34. Pearton SJ, Kang BS, Kim SK, Ren FX, Gila B, Abernathy CR, Lin J, Chu G (2004) GaN-based diodes and transistors for chemical, gas, biological and pressure sensing. J Phys Condens Matter 16:R961–R994

35. Abdulsattar MA (2016) Superlattices Microstruct 93:163–170
36. Khan MS, Srivastava A (2016) J Electroanal Chem 775:243–250
37. Cui H, Yong Y, Jiang H, Yang L, Wang S, Zhang G, Guo M, Li X (2017) Mater Res Express 4:015009
38. Yong Y, Jiang H, Li X, Lv S, Cao J (2016) Phys Chem Chem Phys 18:21431–21441
39. Baik KH, Kim J, Jang S (2017) Sens Actuators B 238:462–467
40. Yong Y, Cui H, Zhou Q, Xiangying Su, Kuangb Y, Li X (2017) Adsorption of gas molecules on a graphitic GaN sheet and its implications for molecule sensors. RSC Adv 7:51027–51035. https://doi.org/10.1039/c7ra11106a
41. Khan MAH (2020) Gallium Nitride (GaN) Nanostructures and their gas sensing properties: a review. Sensors 20:3889. https://doi.org/10.3390/s20143889
42. Kente T, Mhlanga SD (2016) Gallium nitride nanostructures: synthesis, characterization and applications. J Cryst Growth 444:55–72
43. Mollaamin F, Monajjemi M (2023) In silico-DFT investigation of nanocluster alloys of Al-(Mg, Ge, Sn) coated by nitrogen heterocyclic carbenes as corrosion inhibitors. J Clust Sci. https://doi.org/10.1007/s10876-023-02436-5
44. Dural N, Romalis MV (2014) Gallium phosphide as a new material for anodically bonded atomic sensors. APL Mater 2(8). https://doi.org/10.1063/1.4891375.
45. Park K, Lee J, Kim D, Seo J, Kim J, Ahn J-P, Park J (2019) Synthesis of polytypic gallium phosphide and gallium arsenide nanowires and their application as photodetectors. ACS Omega 4(2):3098–3104. https://doi.org/10.1021/acsomega.8b03548
46. Šetka M, Claros M, Chmela O, Vallejos S (2021) Photoactivated materials and sensors for NO2 monitoring. J Mater Chem C 9:16804–16827. https://doi.org/10.1039/D1TC04247E
47. Geng X, Liu X, Mawella-Vithanage L, Hewa-Rahinduwage CC, Zhang L, Brock SL, Tan T, Luo L (2021) Photoexcited NO2 enables accelerated response and recovery kinetics in light-activated NO2 gas sensing. ACS Sens 6:4389–4397. https://doi.org/10.1021/acssensors.1c01694
48. Shin J, Han S, Noh S, Yu Y-T, Kim JS (2021) Room-temperature operation of light-assisted NO2 gas sensor based on GaN nanowires and graphene. Nanotechnology 32:505201. https://doi.org/10.1088/1361-6528/ac2427
49. Pinder RW, Walker JT, Bash JO, Cady-Pereira KE, Henze DK, Luo M et al (2011) Quantifying spatial and temporal variability in atmospheric ammonia with in situ and space-based observations. Geophys Res Lett 38(L04):802. https://doi.org/10.1029/2010GL046146
50. Langridge JM, Lack D, Brock CA, Bahreini R, Middlebrook AM, Neuman JA et al (2012) Evolution of aerosol properties impacting visibility and direct climate forcing in an ammonia-rich urban environment. J Geophys Res-Atmos 117:11. https://doi.org/10.1029/2011jd017116
51. Lamarque JF, Kyle G, Meinshausen M, Riahi K, Smith S, van Vuuren D et al (2011) Global and regional evolution of short-lived radiatively-active gases and aerosols in the representative concentration pathways. Clim Chang 109:191–212
52. Kondratev VM, Kuznetsov A, Fedina SV, Nalimova SS, Moshnikov VA, Bolshakov AD (2022) Gallium phosphide nanowires for "biological concentrations" ammonia detection. J Phys Conf Ser 2172:012006. https://doi.org/10.1088/1742-6596/2172/1/012006
53. Monajjemi M, Mahdavian L, Mollaamin F, Khaleghian M (2009) Interaction of Na, Mg, Al, Si with carbon nanotube (CNT): NMR and IR study. Russ J Inorg Chem 54:1465–1473. https://doi.org/10.1134/S0036023609090216
54. Mollaamin F, Monajjemi M (2023) Molecular modelling framework of metal-organic clusters for conserving surfaces: Langmuir sorption through the TD-DFT/ONIOM approach. Mol Simul 49(4):365–376. https://doi.org/10.1080/08927022.2022.2159996
55. Singh AK, Zhuang HL, Hennig RG (2014) Phys Rev B: Condens Matter Mater Phys 89:245431
56. Dennington R, Keith TA, Millam JM (2016) GaussView. Version 6. Shawnee Mission (KS): Semichem Inc.
57. Frisch MJ, Trucks GW, Schlegel HB, Scuseria GE, Robb MA, Cheeseman JR, Scalmani G, Barone V, Petersson GA, Nakatsuji H et al. (2016) Gaussian 16, Revision C.01, Gaussian, Inc., Wallingford CT
58. Perdew JP, Burke K, Ernzerhof M (1996) Generalized gradient approximation made simple. Phys Rev Lett 77:3865
59. Henkelman G, Arnaldsson A, Jónsson H (2006) A fast and robust algorithm for Bader decomposition of charge density. Comput Mater Sci 36(3):354–360
60. Zhou YG, Zu XT, Gao F et al (2009) Electronic and magnetic properties of graphene absorbed with S atom: a first-principles study. J Appl Phys 105(10):104311
61. Mao Y, Yuan J, Zhong J (2008) Density functional calculation of transition metal adatom adsorption on graphene. J Phys: Condens Matter 20(11):115209
62. Mollaamin F, Monajjemi M (2023) Graphene embedded with transition metals for capturing carbon dioxide: gas detection study using QM methods. Clean Technol 5(1):403–417. https://doi.org/10.3390/cleantechnol5010020
63. Mollaamin F, Shahriari S, Monajjemi M, Khalaj Z (2022) Nanocluster of aluminum lattice via organic inhibitors coating: a study of Freundlich adsorption. J Cluster Science: 1–16. https://doi.org/10.1007/s10876-022-02335-1.
64. Mollaamin F, Monajjemi M (2023) Transition metal (X = Mn, Fe Co, Ni, Cu, Zn)-doped graphene as gas sensor for CO2 and NO2 detection: a molecular modeling framework by DFT perspective. J Mol Model 29:119. https://doi.org/10.1007/s00894-023-05526-3
65. Monajjemi M, Mollaamin F, Gholami MR, Yoosbashizadeh H, Sadrnezhad SK, Passdar H (2003) Quantum chemical parameters of some organic corrosion inhibitors, Pyridine, 2-Picoline 4-Picoline and 2,4-Lutidine, adsorption at aluminum surface in hydrochloric and nitric acids and comparison between two acidic media. Main Group Met Chem 26:349–362. https://doi.org/10.1515/MGMC.2003.26.6.349
66. Svensson M, Humbel S, Froese RDJ, Matsubara T, Sieber S, Morokuma K (1996) ONIOM: A multilayered integrated MO + MM method for geometry optimizations and single point energy predictions. A test for diels−Alder reactions and Pt(P(t-Bu)3)2 + H2 oxidative addition. J Phys Chem 100(50):19357–19363. https://doi.org/10.1021/jp962071j
67. Yanai T, Tew DP, Handy NC (2004) A new hybrid exchange–correlation functional using the Coulomb-attenuating method (CAM-B3LYP). Chem Phys Lett 393(1–3):51–57. https://doi.org/10.1016/j.cplett.2004.06.011
68. Lehtola S (2019) A review on non-relativistic fully numerical electronic structure calculations on atoms and diatomic molecules. Int J Quantum Chem 119(19):25968. https://doi.org/10.1002/qua.25968
69. Smith JAS (1971) Nuclear quadrupole resonance spectroscopy. J Chem Educ 48:39–41
70. Appendix K: Nuclear quadrupole resonance, by Allen N. Garroway, Naval Research Laboratory. In Jacqueline MacDonald, J. R. Lockwood: alternatives for landmine detection. Report MR-1608, Rand Corporation, 2003.
71. Poleshchuck OKh, Kalinna EL, Latosinska JN, Koput J (2001) J Mol Struct (THEOCHEM) 547:233–243
72. Young HA, Freedman RD (2012) Sears and Zemansky's University Physics with Modern Physics, 13th edn. Addison-Wesley, Boston, p 754

73. Fry A, K., D. Kwon, K., Komarneni, S., D. Kubicki, J., T. Mueller, K. (2006) Solid-state NMR and computational chemistry study of mononucleotides adsorbed to alumina. Langmuir 22:9281–9286
74. Kohn W, Becke AD, Parr RG (1996) Density functional theory of electronic structure. J Phys Chem 100:12974–12980. https://doi.org/10.1021/jp960669l
75. Parr RG, Pearson RG (1983) Absolute hardness: companion parameter to absolute electronegativity. J. Am. Chem. Soc 105:7512–7516. https://doi.org/10.1021/ja00364a005
76. Politzer P, Abu-Awwad F (1998) A comparative analysis of Hartree-Fock and Kohn-Sham orbital energies. Theor Chem Acc 99:83–87. https://doi.org/10.1007/s002140050307
77. Silverstein RM, Bassler GC, Morrill TC (1981) Spectrometric Identification of Organic Compounds, 5th edn. Wiley, New York